APL Photonics

Microfluidic devices for quasi-phase-matching in high-order harmonic generation

Cite as: APL Photonics **7**, 110801 (2022); https://doi.org/10.1063/5.0118199
Submitted: 04 August 2022 • Accepted: 30 October 2022 • Accepted Manuscript Online: 31 October 2022 • Published Online: 16 November 2022

A. G. Ciriolo, R. Martínez Vázquez, G. Crippa, et al.

Microfluidic devices for quasi-phase-matching in high-order harmonic generation

Cite as: APL Photon. 7, 110801 (2022); doi: 10.1063/5.0118199
Submitted: 4 August 2022 • Accepted: 30 October 2022 •
Published Online: 16 November 2022

A. G. Ciriolo,[1] R. Martínez Vázquez,[1] G. Crippa,[1,2] M. Devetta,[1] D. Faccialà,[1] P. Barbato,[1,2] F. Frassetto,[3] M. Negro,[1] F. Bariselli,[4] L. Poletto,[3] V. Tosa,[5] A. Frezzotti,[4] C. Vozzi,[1,a)] R. Osellame,[1] and S. Stagira[2]

AFFILIATIONS

[1] National Research Council (CNR), Institute for Photonics and Nanotechnologies, Milano, Italy
[2] Physics Department, Politecnico di Milano, Milano, Italy
[3] National Research Council (CNR), Institute for Photonics and Nanotechnologies, Padova, Italy
[4] Department of Aerospace Science and Technology, Politecnico di Milano, Milano, Italy
[5] National Institute for R&D of Isotopic and Molecular Technologies, Cluj-Napoca, Romania

Note: This paper is part of the APL Photonics Special Topic on Ultrafast Laser Fabrication Enabled Photonics and Devices.
[a)] **Author to whom correspondence should be addressed:** caterina.vozzi@ifn.cnr.it

ABSTRACT

The development of bright eXtreme UltraViolet (XUV) and soft x-ray sources based on high-order harmonic generation is boosting advances toward understanding the behavior of matter on the attosecond timescale. Here, we report a novel approach for efficient XUV generation consisting of the use of microfluidic integrated systems fabricated by femtosecond laser micromachining of glass. Our microfluidic approach allows one to control and manipulate the gas density on a micrometer scale with unprecedented accuracy and micro-structural flexibility. By propagating ultrashort laser pulses inside the microfluidic devices, we demonstrate high photon fluxes and broadband harmonics spectra, up to 200 eV, from tailored gas media.

I. INTRODUCTION

Currently, table-top ultrafast sources of coherent eXtreme UltraViolet (XUV, 10–124 eV) and soft-x-ray (from 124 eV up to a few keV) radiations based on high-order harmonic generation (HHG) are noticeably contributing to scientific advances in understanding the behavior of matter upon electronic excitation on an ultrashort time scale.[1–7] The key point of the success of these sources relies on the unique capability to combine extreme temporal and spatial resolution, allowing the study of ultrafast dynamics with atomic specificity and chemical environment sensitivity down to the attosecond temporal domain (1 as = 10^{-18} s).

In addition to the astonishing potential for unveiling matter dynamics on an extreme time scale, the HG technology is still undergoing continuous progress, intended to overcome several fundamental limits that significantly hinder its applications.

For example, the dramatically low conversion efficiency of HHG still represents a major issue, especially in the soft-x-ray domain, wherein mid-infrared (mid-IR) driving pulses must be used to drive the conversion process. In fact, HHG shows an extremely unfavorable dependence of the yield on the driving pulse wavelength, which scales as λ^{-n} with $5 \leq n \leq 7$.

In this framework, remarkable attention has recently been paid to the development of intense ultrafast near-/mid-IR driving sources at high repetition rates for increasing photon fluence.[8,9] On the other hand, a great effort is currently being devoted to boosting the performances of the HHG sources toward brighter XUV and soft-x-ray emission. Several different configurations have been proposed for enhancing the conversion yield per driving pulse, including HHG in gas-filled capillaries[10] and gas cells.[11]

Capillaries are routinely used in the field of non-linear optics and ultrafast sources for confining the laser beams over longer distances than the Rayleigh range. For instance, gas-filled hollow-core fibers are widely exploited in nonlinear optics[12] and for the compression of intense laser pulses.[13] By combining the benefit of a long-generation medium and a high-energy parametric source, an

extremely bright supercontinuum generation from the XUV up to the keV photon energy was demonstrated by phase-matched emission in a gas-filled capillary driven by millijoule-level mid-IR ultrashort pulses.[14]

For HHG, capillary-based systems are commonly operated in a hydrostatic regime, such that uniform gas densities or shallow pressure gradients can be implemented. The hydrostatic regime ensures a high conversion yield by allowing harmonic emission throughout the entire capillary.[14–17] However, this configuration provides limited control on phase-mismatch and re-absorption by the gas. Re-absorption of XUV radiation from the gas throughout the waveguide becomes extremely critical, and optimal conversion in a long and uniformly dense generation medium is attained over a distance on the scale of the absorption length, provided a coherence longer than the characteristic absorption ($L_{coh} > 5\ L_{abs}$).[18] Moreover, uniformly filled hollow fibers may induce several undesired processes, including long-lived plasma, detrimental to operation at high driving repetition rates,[19] and phase distortion of fundamental pulses due to nonlinear processes such as self-phase modulation.

To date, *Quasi Phase Matching* (QPM) by a periodic corrugation of the fiber inner diameter for modulating the laser peak intensity[20,21] provides the experimental demonstration of enhanced harmonic generation yield by control of the capillary geometry on a sub-millimeter scale.

However, the coherent growth of the XUV radiation in capillaries is sensitive to any perturbation of the driving field due to radiative losses during the propagation and dispersion in the neutral and ionized gas and mode-beating.[22] Thus, the phase-matching condition might significantly change along the propagation,[23] requiring a local adjustment of the periodicity to recover in-phase dipole emission. HHG in aperiodic configurations to increase QPM emission of selected harmonics has been theoretically proposed,[24–26] but not experimentally demonstrated yet, mainly due to the technical difficulties associated with control and optimization of the waveguide microstructure.

In this framework, the remarkable advances in micromachining techniques offer novel perspectives to coherent nonlinear conversion processes. In fact, the availability of microfluidic systems allows tailoring of both the capillary shape and gas density modulation, thus enabling control of the generation medium, well beyond the hydrostatic regime.

We propose a novel approach to XUV generation and manipulation based on microfluidic glass devices, which is intended to combine the benefits of microfluidics with ultrafast nonlinear optics in hollow-core fibers.

We exploit the *Femtosecond Laser Irradiation followed by Chemical Etching* (FLICE) micromachining technique to build embedded hollow three-dimensional structures in the bulk of glass substrates.[27–29] We use these microstructured devices as microfluidic systems for fine control of the gas density in the laser–gas interaction volume. We measured the efficient XUV generation in the 40–190 eV spectral range and showed the possibility to manipulate and control the phase-matching conditions by tailoring the gas density with micrometer accuracy. In particular, we demonstrate, for the first time, the generation of harmonics in periodic and aperiodic gas density modulations through an array of multi-jets inside a hollow waveguide. This approach is suitable for more complex engineering with unprecedented flexibility and marks a promising route to high-brightness tabletop ultrafast microfluidic-based XUV sources.

II. MICROFLUIDIC SOURCES FOR HHG

The archetypal structure of our devices is composed of a hollow-core waveguide and a microfluidic module for gas delivery and manipulation integrated into a monolithic finger-top glass chip engineered to work in a vacuum environment.

As we already reported in our previous work,[30] the concept of those devices is inspired by the capillary scheme and works under a vacuum environment in a continuous gas flow regime.

The devices are fabricated by the FLICE technique, which consists of irradiating fused silica (FOCtek Photonics) substrates ($1 \times 10 \times 8\ mm^3$) by high repetition rate femtosecond pulses. In the focal volume, a high amount of energy is deposited, inducing a permanent modification of the material, which becomes locally more sensitive to the chemical attack by an etchant solution. The standard design of a device consists of a 100 μm-deep rectangular-like thin reservoir ($2 \times 4.7 \times 0.1\ mm^3$) from which an arrangement of microchannels departs, distributing the gas into the hollow-core waveguide, which is 8 mm long and has a diameter of 130 μm. Specifically, four evenly distributed injection micro-pipes with a cylindrical shape, arranged at a distance of 1.2 mm from each other to cover the entire area of the reservoir, are used to achieve a uniform gas distribution along the waveguide. Fig. 1(a) provides a scheme of the device.

The gas, injected by the microfluidic module, flows through a few-mm-long hollow waveguide under the pressure gradient downstream of the capillary extremities. In these devices, the flow is almost isothermal, with the density profile being proportional to the pressure, which smoothly varies from the center to the outputs of the waveguide, thus giving a central region with a constant density profile.[31]

A. Photon flux and conversion efficiency of the microfluidic source

To drive HHG, we used pulses at 800 nm wavelength delivered by an amplified Ti: Sapphire laser source (Amplitude, Aurora laser system: 15 mJ, 25 fs, 1 kHz). The laser pulses for this experiment were 25 fs long (Full Width at Half Maximum—FWHM—of the pulse intensity envelope) and with an energy of 500 μJ. The pulses are focused into the devices by a lens with a 30 cm focal length, matched for coupling the EH11 hybrid mode.[32] The alignment of the device is performed by a high-precision multi-axes motorized translational system inside a vacuum chamber. A view of the HHG setup is shown in Fig. 1(b).

The gas is delivered to the device by a pipeline that is directly interfaced with the mechanical mounting that contains the chip. The gas density can be manually tuned by a needle valve mounted upstream of the gas pipeline, and the backing pressure is accurately monitored by a capacitive pressure gauge placed after the valve. The working pressure in the generation chamber ranges between 10^{-4} and 10^{-5} mbar depending on the measured gas backing pressure.

Here, we show a characterization of the performances of the microfluidic source by photon flux and conversion efficiency. In Fig. 1(c), we report HHG spectra generated in argon and helium.

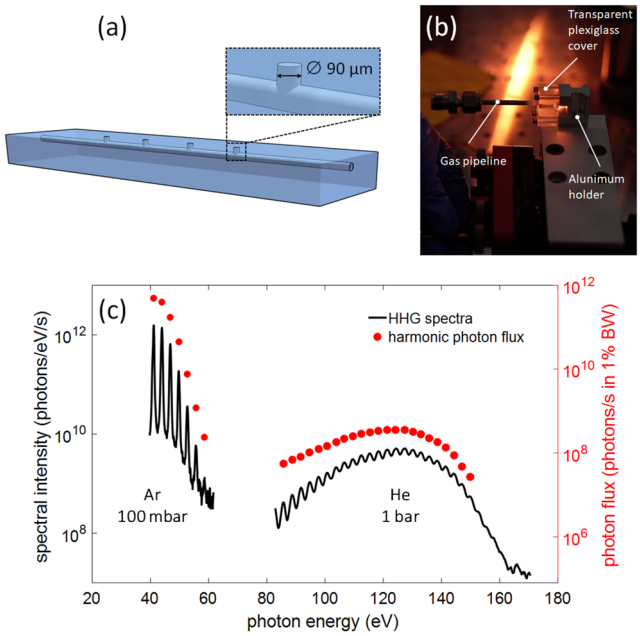

FIG. 1. XUV generation in microfluidic devices. (a) Picture of a microfluidic device for HHG. The mounting of the device is shown in figure (b). It is composed of an aluminum holder and Plexiglass, the chip being encapsulated in-between. A Viton gasket is used for sealing. The gas is delivered through a pipeline directly connected to the Plexiglass cover. The mounting is placed on a high-precision motorized translational stage. (c) HHG spectra generated in a glass device composed of 8 mm long capillary. The argon spectrum is generated at a backing pressure of 100 mbar, and the helium spectrum at a backing pressure of 1 bar. The acquisition time is 1 s for the spectrum generated in argon and 5 s for the one generated in helium. On the right axis, in red, the corresponding photon flux per second in 1% bandwidth is reported. Picture (b) courtesy of Simone Campanella.

With argon, the generation yield is maximized at a backing pressure of 100 mbar. In these conditions, harmonics up to 60 eV were generated. We measured peak photon flux approaching 10^{12} photons/s in 1% bandwidth at 41 eV, corresponding to a conversion efficiency of $8 \cdot 10^{-6}$ in 1% bandwidth. Compared to capillary-based XUV sources operated under similar experimental conditions (1 cm capillary filled with 120 mbar of Ar, 400 μJ Ti: Sa pulses at 1 kHz repetition rate),[17] the microfluidic source shows an enhanced photon flux of almost two orders of magnitude.

To date, higher photon fluxes, up to 10^{13} photons/s in 1% bandwidth, were generated in the spectral region of 30–40 eV through HHG in continuous gas-jet driven by μJ-level high-repetition-rate sources, operating from 10 kHz to 10 MHz.[33–35] Bright XUV generation in a gas cell driven by multi-millijoule 10 Hz driving laser sources was also reported, providing photon fluxes up to $6 \cdot 10^{12}$ photons/s in 1% bandwidth at the range of 20–30 eV.[36–38] In addition to HHG by single-pass on gas targets, multi-MHz cavity-enhanced HHG technology driven by high average power lasers has recently experienced huge advances in photon fluxes delivery in the spectral range between 20 and 60 eV.[19,39–41] However, single-pass HHG still outperforms the efficiencies of cavity-enhanced generation systems, mainly because of intra-cavity phase instabilities and detrimental cumulative plasma effects inside the generation volume that might hinder the in-cavity process.[19,42]

To frame the performances of our microfluidic system with the state-of-the-art HHG XUV and soft-x-ray sources, we compare the conversion efficiency per driving pulse energy as a function of the generated photon energies in Fig. 2. By inspection, we find that the XUV generation efficiency in argon is in line with that of the most efficient XUV sources reported in the literature so far.

Efficient HHG in helium by the microfluidic source required a higher backing pressure of 1 bar. The harmonics spectrum ranged from 80 up to 150 eV, with a photon flux larger than 10^7 photons/s in 1% bandwidth within the whole spectral range, and a peak value of $8 \cdot 10^8$ photons/s in 1% bandwidth at 130 eV, corresponding to a conversion efficiency of $1.8 \cdot 10^{-8}$ in 1% bandwidth. We observed an improvement in the photon flux by increasing the backing pressures, with a favorable indication of non-detrimental absorption. However, the pressure range we could access so far did not allow photon flux optimization in the microfluidic cell, since the maximum baking pressure was limited by the vacuum pumping system to 1 bar, at continuous gas flow. The device can operate in a multi-bar regime, but differential pumping is needed to apply pressures above 1 bar.

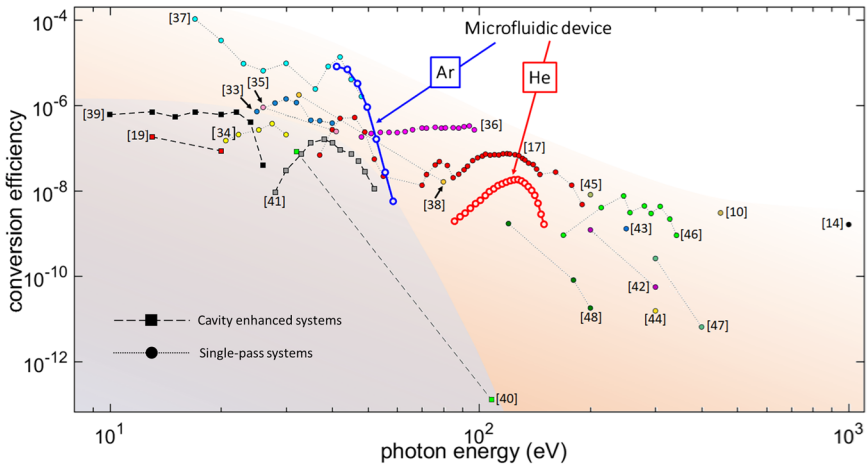

FIG. 2. State of the art in HHG-based XUV and soft-x-ray sources. The graph shows the conversion efficiency in 1% bandwidth. If not directly provided, the 1%-BW conversion efficiency was estimated from the data and experimental parameters reported in the manuscripts. Circles mark single-pass HHG, and squares mark cavity-enhanced HHG. The shaded areas define the conversion efficiency range covered by single-pass (light red) and cavity-based (light blue) sources.

For photon energies above 100 eV, near- and mid-IR (1.5–4 μm) ultrashort pulses are routinely exploited to drive HHG.[10,14,42–47] This leads to a dramatic drop in the conversion efficiency of single-pass schemes due to the unfavorable scaling with fundamental driving wavelength. In this framework, scaling the system to higher gas densities is a fundamental requirement for efficient XUV emission in the water window.[48] In fact, the suppression of the single-atom yield at long driving wavelengths can be partially counterbalanced by a favorable phase-matching in the multi-bar regime and by increased transparency at photon energies approaching the keV,[10,14] allowing enhanced conversion efficiency by coherent superposition from highly dense and long gas media.

In this sense, the microfluidic sources provide a suitable technology for enabling both beam confinement in hollow waveguides and high local gas densities. Furthermore, they ensure the unique capability to accurately control and manipulate the gas distribution for tailored phase-matching conditions, as shown in Sec. III.

III. MULTI-NOZZLE MICROFLUIDIC SOURCES FOR HHG IN A QPM REGIME

The coherent build-up of harmonics through QPM based on structured gas density distribution was theoretically proposed by Auguste *et al.*[49] The experimental demonstration of this effect has been reported by Seres *et al.*[51] In their work, the modulation of the gas density was obtained by adding two gas sources in a focused laser beam. However, in a tight-focusing geometry, scaling this scheme to a larger number of gas sources is challenging. Furthermore, based on the theoretical work by Hadas and Bahabad,[51] on HHG in a shallow focusing regime, the nonlinear optical conversion by QPM in a periodically modulated gas medium may be strongly inefficient. This result suggests investigating the possibility to overcome the theoretical limitations of a periodic geometry by the use of a nonperiodic gas density modulation.

In this framework, we developed microfluidic devices equipped with a more sophisticated gas-delivery module, composed of an array of identical De Laval micronozzles, whose supersonic outflow improves the spatial focusing of the gas sources at the inlets of the main channel. These micronozzles are directly interfaced with the hollow waveguide, such that local gas density peaks can be realized along the beam path. The tailoring of the gas density in this kind of device can be engineered by changing the shape, the number, and the position of the micronozzles.

A. HHG with integrated arrays of gas jets

The micronozzles are characterized by a convergent–divergent profile with diameters of 220, 60, and 90 μm in the input, throat, and output, respectively. The convergent zone has a length of 55 μm, and the divergent one of 75 μm. We realized two different multi-jet microfluidic sources, the first composed of four evenly distributed gas jets (relative distance L = 1.2 mm), and the second composed of three gas jets accommodated at different relative distances (L1 = 1.9 mm and L2 = 1.4 mm). In front of the nozzle outlets, we arranged an exhaust rectangular opening to allow free gas expansion and to reduce gas stagnation between two adjacent gas jets. To preserve the optical structure of the hollow waveguide, the width of the opening was set at 90 μm, smaller than the diameter of the waveguide. A scheme of the two layouts is reported in Fig. 5(a).

In these devices, we obtained focused and confined gas jets, providing the desired gas density peaks along the waveguide axis. In both configurations (with three and four nozzles), we arranged the gas jets at a distance much larger than their transversal size to obtain a high gas density contrast between the jets and the background. The geometry was preliminarily optimized by running computational fluid dynamics (CFD) simulations. The Navier–Stokes–Fourier (NSF)[52] equations for a viscous and compressible fluid were used to study the steady gas flow through the device. NSF equations were solved numerically on the commercial Comsol Multiphysics™ CFD platform.[53] A laminar flow regime was assumed due to the relatively low value of the reference Reynolds number. No-slip boundary conditions were applied to walls due to the small value of the Knudsen number[54] in the whole flow domain. Details about the adopted grid structure are given in the supplementary material (Sec. S1). Under these conditions, a moderately supersonic gas flow inside the waveguide is obtained at the output of the nozzles.

Figure 3(b) reports a sectional view of the numerical gas density distributions computed at a backing pressure in the reservoir of 1 bar. The gas distribution is composed of highly dense and confined gas jets interposed to the low-density background, with a high peak-to-background contrast ratio: the density contrast is >7 in the middle of the waveguide, while it is >20 on the two extremities of the waveguide. Under these conditions, we can minimize the contribution to HHG from the gas background and can study the dependence of the harmonic emission on the gas density modulation by directly comparing the harmonics spectra in different gas-jets configurations.

The use of two different devices with three and four nozzles required changing the device from one measurement to the other and aligning them independently. To allow for a reliable comparison of HHG in the two configurations, we constantly checked the laser parameters (energy, spectrum, pulse compression) and the coupling efficiency (output power over input power) to be stable from one measurement to the other. The beam coupling inside the devices is monitored by an auxiliary beamline equipped with a mirror mounted on a motorized translational stage that can be inserted into the beamline to send the output mode onto a beam profiler. Moreover, we used to make a precise adjustment of the beam-to-device alignment through the remotely controlled five-axis motion system, by direct optimization of the harmonic signal.

Figure 4 shows the experimental high-order harmonic spectra generated in the two devices filled with helium at a backing pressure of 1 bar. A clear difference between the two spectra can be observed throughout the whole spectral range. In fact, the yield is not monotonically related to the number of sources, but it exhibits a counterintuitive re-shaping. In the three-jet aperiodic configuration, we observe a higher generation yield at the cutoff. In fact, in the periodic four-nozzles arrangement, harmonic components up to 140 eV are efficiently generated, while, in the aperiodic three-jets arrangement, the spectrum approaches 200 eV, with an exponential decrease of the harmonic intensity above the cutoff, at 190 eV.

A phenomenological picture of the mechanism behind the yield enhancement of selected portions of the XUV spectrum induced by phase matching can be drawn in terms of the coherence length of the harmonic components.

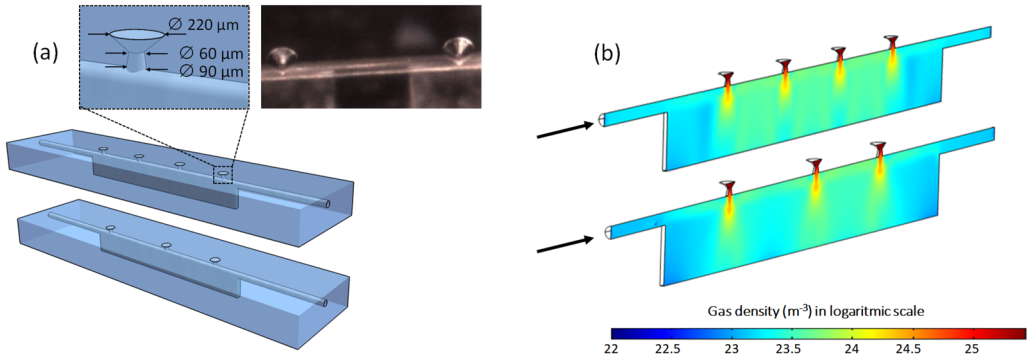

FIG. 3. HHG in the multi-jet devices. (a) Structure of devices with multi-jets for HHG. The blow-up on the left shows the nozzle structure, and the blow-up on the right provides a microscope view of a portion of a device equipped with nozzles. Microscope view of a portion of the device where you can see the micronozzles and the hollow-core waveguide. (b) We report a sectional view of the simulated gas density (m^{-3}) in the devices with four and three nozzles. The black arrow indicates the laser entrance direction.

Since the gas jets are very confined in space along the waveguide axis, with a longitudinal length of ~100 μm, they can be considered as point sources of harmonics emission. During the propagation from one nozzle to the next one, the harmonics radiation undergoes dephasing from the fundamental field because of the dispersion produced by the residual gas background inside the waveguide. This dephasing is quantified by the phase-mismatch parameter Δk_q. The coherence length of the q-th harmonic component is related to Δk_q according to the following definition, $L_{c,q} = 2\pi/\Delta k_q$. In a simple picture, point sources that are exactly placed at a distance of $n \cdot L_{c,q}$ are perfectly matched in phase for the q-th harmonic component, and a constructive sum of their emission occurs. A deviation from ideal conditions might result in significant suppression of the spectral intensity of specific spectral regions.

A one-dimensional propagation model intended to give a description of the harmonic field propagation along the waveguide is reported in Sec. III B.

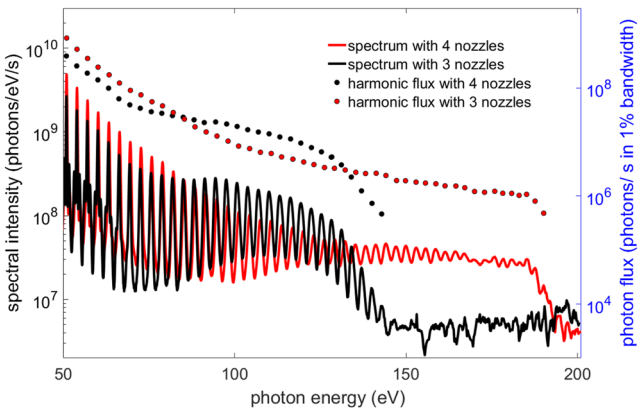

FIG. 4. HHG spectra and photon fluxes (blue axis) generated in helium by the device with four evenly distributed nozzles (black) and three aperiodic nozzles (red) using a backing pressure of 1 bar. The acquisition time of the spectra is 5 s.

B. A simple-man 1D propagation model of HHG in a multi-jet

To investigate the growth of the harmonic components at higher energies in a tailored gas density, we calculate the phase-mismatch Δk_q between the fundamental and harmonic fields for each harmonic order q. We used a one-dimensional approximation, in which we assumed the fundamental coupled to the EH11 mode of the hollow waveguide. The pulse is modeled in the temporal domain as a Gaussian envelope with a Full width at Half Maximum (FWHM) duration and intensity of 25 fs and $9.5 \cdot 10^{14}$ W/cm^2, respectively. Due to the short propagation distance, we neglected the radiative losses through the hollow waveguide boundaries. The ionization fraction η was estimated by the Yudin and Ivanov model,[55] leading to $\eta_p = 5.9\%$ at the pulse peak in helium.

In the model, we assumed the fundamental pulse to propagate in a medium with a constant ion fraction η_p within the full length of the waveguide. The phase mismatch for the q-th harmonic is written as[15]

$$\Delta k_q(x) = -\frac{q{u_{11}}^2\lambda_0}{4\pi a^2} + k_0 q\left[(n_o(\rho) - n_q(\rho))(1-\eta_p) - \frac{\rho}{\rho_{atm}}\eta_p\frac{{\omega_p}^2}{{\omega_0}^2}\left(1-\frac{1}{q^2}\right)\right],$$

where ρ_{atm}, a, u_{11}, k_0, ω_0, and ω_p represent the gas density (in standard conditions), the waveguide radius, the first zero of the Bessel function J_0, the fundamental wavevector, the fundamental frequency, and the plasma frequencies for a fully ionized gas at 1 *atm* in standard conditions, respectively. $n(\rho)$ and $nq(\rho)$ are the refractive indices calculated as a function of the local gas density $\rho(x)$. x is the laser propagation direction.

The harmonic field is computed by solving numerically the growth equation,[51]

$$\frac{dE_q}{dx} = -\alpha_q(x)E_q + b(x)e^{i\int_{-x_0}^{x}\Delta k_q(x')dx'},$$

where α_q is the medium absorption as a function of the gas density distribution and $b(x) = iq\omega_0{}^2\rho(x)d_q(x)\ (1 - \eta_p)/2\varepsilon_0 c_0$. The second term is the polarization field of the q-th order. To isolate the role of the phase mismatch in the development of the harmonic field, the nonlinear dipole moment $d_q(x)$ is assumed to be constant along x for each harmonic order.

To take into account the three-dimensional gas density distribution inside the waveguide, the 1D model was applied along the waveguide axis on a bundle of lines parallel to the waveguide axis and regularly distributed inside the waveguide volume.

Specifically, for sampling the gas density $\rho(x,y,z)$, we divided the 3D waveguide volume into a discrete number of n sub-volumes, with $n = 44$, that form a Cartesian grid. Each sub-volume has a squared base with $\Delta y \cdot \Delta z = (R/4)^2$ ($\Delta y = \Delta z = R/4$, R waveguide radius) and a length of 8 mm (waveguide length). For each point along x, we extrapolated the average density value within the sub-volumes and obtained a set of n gas density profiles that accounts for the non-uniform gas distribution along different axial lines with fixed (y_n,z_n)-coordinates inside the waveguide, $\rho_n(x)$. We used the $\rho_n(x)$ profiles to calculate the harmonic field along x in each n-th domain, according to the above-mentioned dE_q/dx equation. The phase-mismatch parameter $\Delta k_q(x)$ is density-dependent, thus providing different phase field conditions depending on n. To account for the non-uniform electric field intensity on the (y,z) planes, we calculated the driving field amplitude E_n and the corresponding nonlinear dipole moment $d_{q,n}$ for each n-th volume by assuming a Bessel-like radial profile for the field mode inside the waveguide (EH11). By applying the corresponding n-th input conditions on gas density and driving field amplitude, we obtained a set of harmonic spectra and summed them to obtain the final HHG spectrum.

Figure 5(a) shows the numerical HHG spectra calculated from the single-atom nonlinear dipole[56] by applying to each harmonic component an amplitude modulation according to the above-described phase-matching model for the two different nozzle distributions, with three (red curve) and four (black curve) jets.

The model reproduced well the enhancement of the cutoff yield in the three-nozzle configuration compared to the four-nozzle case. The nonlinear field growth along the propagation direction as a function of the harmonic order as predicted by this simple-man model for harmonics 95 (147 eV) and 109 (169 eV) is shown in Figs. 5(c) and 5(d), respectively.

The fields have a characteristic step-like behavior in correspondence to the gas peaks, overlapped with periodic amplitude modulation. The modulation is due to the residual gas background inside the waveguide, and the periodicity is related to the effective coherence length of the harmonic as they propagate in the residual gas. The gas density peaks produce a change in both the harmonic amplitude. In particular, the phase accumulated by the q-th harmonic during the propagation in the gas background may induce destructive or constructive interference with the newly generated field inside the gas jet. This results in a local increase or a decrease in the amplitude of the up-converted field, depending on the gas jet position. The four-nozzle scheme allows a favorable field growth in the range of 140–150 eV, while it provides a less favorable quasi-phase-matching for harmonics between 160 and 200 eV. Due to the different inter-nozzle distances, phase-matching is achieved on a broader spectral region in the three-nozzle device. If the growth of a harmonic component between two jets is hindered because of an unfavorable jet distance, phase-matching can be recovered by detuning the distance of the third jet. Thus, the components at the cutoff are not suppressed and a higher conversion yield is measured in this spectral region. We estimated that in both devices, the role of absorption in the gas-jet configurations is negligible, leading to an attenuation of less than 5% of the harmonic field.

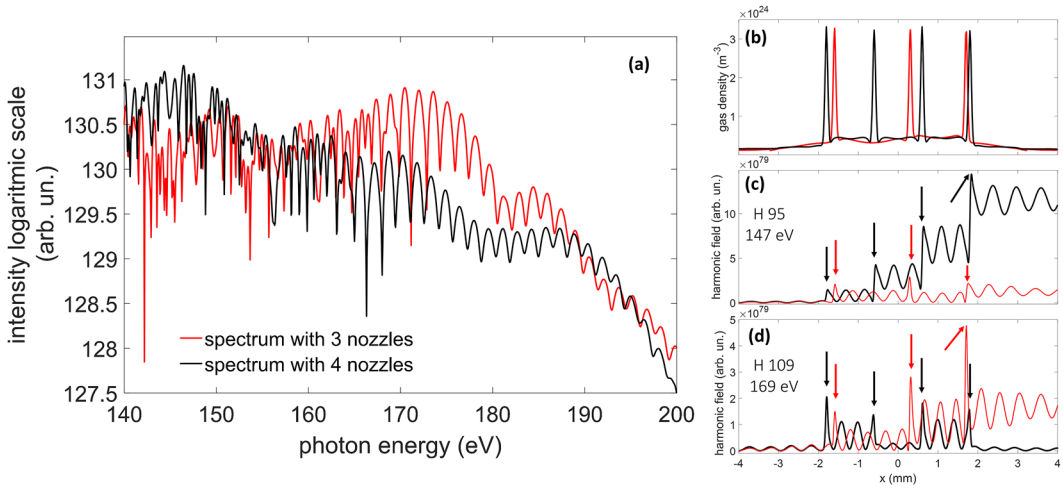

FIG. 5. Computed harmonic field in a modulated gas density. (a) Numerical HHG spectra of the three-nozzle (red) and four-nozzle (black) configurations. (b) Numerical gas density profile for the three (red) and four (black) gas jets along the waveguide axis. The axial profile was extrapolated from the 3D numerical calculations. (c) and (d) show the growth of the harmonic field along the waveguide axis with the two different gas density distributions for harmonics 95 and 109, respectively. The red and black arrows indicate the position of the gas density peaks.

IV. CONCLUSIONS AND PERSPECTIVES

We demonstrated efficient XUV generation and quasi-phase-matching control inside microfluidic devices fabricated by the FLICE technique. Our microfluidic source provides a conversion efficiency in line with the state-of-the-art table-top XUV sources based on HHG. Compared to HHG in static gas cells and gas-filled waveguides, the microfluidic approach offers the unique advantage of enabling micro-manipulation of the gas distribution within the generation volume, thus allowing accurate control and shaping of the harmonic generation conditions. In this framework, we showed XUV generation by gas density modulation in a periodic and aperiodic micro-jets arrangement. The difference in both the HHG yield and cut-off measured within the two different arrangements demonstrates the possibility to tune phase-matching in a selected portion of the spectrum by the nozzle position. This approach is scalable to multi-bar backing pressures and more complex gas jet architectures, including a higher number of nozzles and customized spatial positioning.

A promising development of our microfluidic technology includes the remote control of moving parts by vacuum-compatible micro-actuators for blocking the gas supply to each nozzle independently. Reconfiguring the nozzle array inside the same device could be possible through the integration of optical switches based on thermos-optic or piezo-electric effects.[57]

Following the route traced by microfluidics, we foresee the realization of innovative platforms for XUV/x-ray science inspired by the concept of lab-on-a-chip (LOC). To date, LOCs are widely exploited for biomedical, chemical, and environmental purposes,[58–60] herein mainly applied to the manipulation of liquids. However, they are perfectly suitable for the transport of gases as well. Moreover, despite recent progress in x-ray transport and focusing produced by the advances in diffractive, refractive, and guided optics,[61,62] the optical technology behind HHG beamlines remains extremely complex and, thus, restrained to few advanced laboratories.

In this sense, our approach provides a first demonstration of the potential for extending the concept of LOC to x-ray beamlines. By reversing the paradigm of large-scale facilities for x-ray science, we envisage the possibility to realize miniaturized microfluidic experimental stations, taking advantage of the impressive capabilities of the FLICE technique. In fact, such an integrated microfluidic scheme can be extended to encompass more complex optical functionalities, including the interaction with either gas or liquid samples as well as the handling of multiple laser beams by pulse splitting, delay lines, and interferometers,[63] thus forwarding the perspective of a new generation of lab-on-a-chip for attosecond spectroscopy and x-ray-based technologies.

V. MATERIALS AND METHODS

The fabrication of the glass devices begins with the irradiation of the fused silica slab with a focused femtosecond laser beam (Satsuma HP, Amplitude), with a repetition rate of 1 MHz, 230 fs pulse duration, and pulse energy of 300 nJ. We used the second harmonic (515 nm) of the laser beam and focused it inside the glass slab by a 63× microscope objective (0.65 NA) endowed with a correction ring (LD-Plan Neofluar, Zeiss). The sample is moved with respect to the laser beam, thanks to a three-axis stage (200 nm resolution ANT stages, Aerotech), following the desired trajectory. Then, the sample is immersed for 2–3 h into a 20% aqueous solution of hydrofluoric acid (HF) in an ultrasonic bath at 35 °C to remove the irradiated regions and reveal the desired empty channels.

The main characteristic of the FLICE technique is the possibility of combining in the same device three-dimensional empty structures with arbitrary profiles and different dimensions (from micrometer to millimeter), such as the micronozzles and the hollow waveguide. To succeed in it, the irradiated pattern has been engineered to compensate for inhomogeneous exposition to acid during the etching step. This allows for achieving a central channel with a constant radius and De Laval nozzles with desired dimensions.

The grazing incidence XUV spectrometer used for collecting the HHG radiation works in a stigmatic configuration.[64] The HHG signal is dispersed by a grazing incidence grating (Hitachi, working range of 5–100 nm) and detected by a Micro-Channel Plate (MCP) followed by a phosphor screen. The image displayed on the phosphor screen is acquired by a CCD camera (Andor, Apogee Ascent A1050). The photon flux was measured by a low-noise air-cooled CCD camera (PIXIS-XO 2048B, Princeton Instrument) mounted in the focal plane of the spectrometer in place of the MCP and working in the x-ray range between 10 eV and 30 keV. To remove the co-propagating fundamental beam, we used metallic filters (110 nm Al filter for HHG in argon, 150 nm Pd filter for HHG in helium). The photon number per pulse is obtained by accounting for the absorption of the metal filters,[65] the grating efficiency of the XUV spectrometer,[66] and the quantum efficiency of the camera.[67]

SUPPLEMENTARY MATERIAL

See supplementary material for additional details about the microfluidic simulations and additional experimental results on high-order harmonics generated in chips with nozzles as a function of the gas pressure.

ACKNOWLEDGMENTS

We thank Amplitude and Dr. Philippe Demengeot for their support. This project has received funding from the European Unions Horizon 2020 Research and Innovation Program under Grant Agreement No. 964588 (XPIC), the European Research Council Proof of Concept Grant FESTA (Grant No. 813103) and MSCA-ITN SMART-X (Grant No. 860553), the European COST Action Grant No. CA18222 (AttoChem), the Italian Ministry of Research and Education with the projects ELIESFRI Roadmap and PRIN aSTAR (Grant No. 2017RKWTMY), and the Consiglio Nazionale delle Ricerche with the Joint Laboratory ATTOBIO.

AUTHOR DECLARATIONS

Conflict of Interest

The authors have no conflicts to disclose.

Author Contributions

A.G.C. and R.M.V. contributed equally to this work.

A. G. Ciriolo: Data curation (lead); Formal analysis (lead); Investigation (lead); Methodology (equal); Software (equal); Validation (equal); Visualization (equal); Writing – original draft (equal); Writing – review & editing (equal). **R. Martínez Vázquez**: Formal analysis (lead); Funding acquisition (equal); Investigation (lead); Methodology (equal); Project administration (equal); Resources (equal); Supervision (equal); Validation (equal); Visualization (equal); Writing – original draft (equal); Writing – review & editing (equal). **G. Crippa**: Data curation (supporting); Formal analysis (supporting); Investigation (equal); Software (equal); Writing – review & editing (supporting). **M. Devetta**: Funding acquisition (equal); Investigation (supporting); Resources (supporting); Software (equal); Writing – review & editing (supporting). **D. Faccialà**: Formal analysis (supporting); Investigation (supporting); Methodology (equal); Software (equal); Writing – review & editing (supporting). **P. Barbato**: Investigation (supporting); Resources (equal); Writing – review & editing (supporting). **F. Frassetto**: Resources (supporting); Writing – review & editing (supporting). **M. Negro**: Investigation (supporting); Writing – review & editing (supporting). **F. Bariselli**: Methodology (equal); Writing – review & editing (supporting). **L. Poletto**: Resources (supporting); Writing – review & editing (supporting). **V. Tosa**: Methodology (supporting); Writing – review & editing (supporting). **A. Frezzotti**: Methodology (supporting); Supervision (equal); Writing – review & editing (supporting). **C. Vozzi**: Conceptualization (equal); Funding acquisition (equal); Project administration (equal); Supervision (equal); Validation (equal); Writing – review & editing (equal). **R. Osellame**: Conceptualization (equal); Funding acquisition (equal); Writing – review & editing (supporting). **S. Stagira**: Conceptualization (equal); Funding acquisition (equal); Project administration (equal); Supervision (equal); Validation (equal); Writing – review & editing (equal).

DATA AVAILABILITY

The data that support the findings of this study are available from the corresponding author upon reasonable request.

REFERENCES

[1] F. Calegari, D. Ayuso, A. Trabattoni, L. Belshaw, S. De Camillis, S. Anumula, F. Frassetto, L. Poletto, A. Palacios, P. Decleva, J. B. Greenwood, F. Martín, and M. Nisoli, "Ultrafast electron dynamics in phenylalanine initiated by attosecond pulses," Science **346**, 336–339 (2014).

[2] M. Schultze, K. Ramasesha, C. D. Pemmaraju, S. A. Sato, D. Whitmore, A. Gandman, J. S. Prell, L. J. Borja, D. Prendergast, K. Yabana, D. M. Neumark, and S. R. Leone, "Attosecond band-gap dynamics in silicon," Science **346**, 1348–1352 (2014).

[3] T. T. Luu, M. Garg, S. Y. Kruchinin, A. Moulet, M. T. Hassan, and E. Goulielmakis, "Extreme ultraviolet high-harmonic spectroscopy of solids," Nature **521**, 498–502 (2015).

[4] A. Sommer, E. M. Bothschafter, S. A. Sato, C. Jakubeit, T. Latka, O. Razskazovskaya, H. Fattahi, M. Jobst, W. Schweinberger, V. Shirvanyan, V. S. Yakovlev, R. Kienberger, K. Yabana, N. Karpowicz, M. Schultze, and F. Krausz, "Attosecond nonlinear polarization and light–matter energy transfer in solids," Nature **534**, 86–90 (2016).

[5] M. T. Hassan, T. T. Luu, A. Moulet, O. Raskazovskaya, P. Zhokhov, M. Garg, N. Karpowicz, A. M. Zheltikov, V. Pervak, F. Krausz, and E. Goulielmakis, "Optical attosecond pulses and tracking the nonlinear response of bound electrons," Nature **530**, 66–70 (2016).

[6] D. M. Villeneuve, P. Hockett, M. J. J. Vrakking, and H. Niikura, "Coherent imaging of an attosecond electron wave packet," Science **356**, 1150–1153 (2017).

[7] Y. Kobayashi, K. F. Chang, T. Zeng, D. M. Neumark, and S. R. Leone, "Direct mapping of curve-crossing dynamics in IBr by attosecond transient absorption spectroscopy," Science **365**, 79–83 (2019).

[8] U. Elu, M. Baudisch, H. Pires, F. Tani, M. H. Frosz, F. Köttig, A. Ermolov, P. S. Russell, and J. Biegert, "High average power and single-cycle pulses from a mid-IR optical parametric chirped pulse amplifier," Optica **4**, 1024–1029 (2017).

[9] U. Elu, T. Steinle, D. Sánchez, L. Maidment, K. Zawilski, P. Schunemann, U. D. Zeitner, C. Simon-Boisson, and J. Biegert, "Table-top high-energy 7 μm OPCPA and 260 mJ Ho:YLF pump laser," Opt. Lett. **44**, 3194–3197 (2019).

[10] M.-C. Chen, P. Arpin, T. Popmintchev, M. Gerrity, B. Zhang, M. Seaberg, D. Popmintchev, M. M. Murnane, and H. C. Kapteyn, "Bright, coherent, ultrafast soft x-ray harmonics spanning the water window from a tabletop light source," Phys. Rev. Lett. **105**, 173901 (2010).

[11] J. Peatross, J. R. Miller, K. R. Smith, S. E. Rhynard, and B. W. Pratt, "Phase matching of high-order harmonic generation in helium-and neon-filled gas cells," J. Mod. Opt. **51**, 2675–2683 (2004).

[12] A. G. Ciriolo, A. Pusala, M. Negro, M. Devetta, D. Faccialà, G. Mariani, C. Vozzi, and S. Stagira, "Generation of ultrashort pulses by four wave mixing in a gas-filled hollow core fiber," J. Opt. **20**, 125503 (2018).

[13] M. Nisoli, S. De Silvestri, and O. Svelto, "Generation of high energy 10 fs pulses by a new pulse compression technique," Appl. Phys. Lett. **68**, 2793–2795 (1996).

[14] T. Popmintchev, M.-C. Chen, D. Popmintchev, P. Arpin, S. Brown, S. Ališauskas, G. Andriukaitis, T. Balčiunas, O. D. Mücke, and A. Pugzlys, "Bright coherent ultrahigh harmonics in the keV x-ray regime from mid-infrared femtosecond lasers," Science **336**, 1287–1291 (2012).

[15] C. G. Durfee III, A. R. Rundquist, S. Backus, C. Herne, M. M. Murnane, and H. C. Kapteyn, "Phase matching of high-order harmonics in hollow waveguides," Phys. Rev. Lett. **83**, 2187 (1999).

[16] X. Zhang, A. Lytle, T. Popmintchev, A. Paul, N. Wagner, M. Murnane, H. Kapteyn, and I. P. Christov, "Phase matching, quasi-phase matching, and pulse compression in a single waveguide for enhanced high-harmonic generation," Opt. Lett. **30**, 1971–1973 (2005).

[17] C. Ding, W. Xiong, T. Fan, D. D. Hickstein, T. Popmintchev, X. Zhang, M. Walls, M. M. Murnane, and H. C. Kapteyn, "High flux coherent supercontinuum soft X-ray source driven by a single-stage, 10 mJ, Ti:sapphire amplifier-pumped OPA," Opt. Express **22**, 6194–6202 (2014).

[18] E. Constant, D. Garzella, P. Breger, E. Mével, C. Dorrer, C. Le Blanc, F. Salin, and P. Agostini, "Optimizing high harmonic generation in absorbing gases: Model and experiment," Phys. Rev. Lett. **82**, 1668 (1999).

[19] G. Porat, C. M. Heyl, S. B. Schoun, C. Benko, N. Dörre, K. L. Corwin, and J. Ye, "Phase-matched extreme-ultraviolet frequency-comb generation," Nat. Photonics **12**, 387–391 (2018).

[20] E. A. Gibson, A. Paul, N. Wagner, D. Gaudiosi, S. Backus, I. P. Christov, A. Aquila, E. M. Gullikson, D. T. Attwood, M. M. Murnane, and H. C. Kapteyn, "Coherent soft x-ray generation in the water window with quasi-phase matching," Science **302**(5642), 95–98 (2003).

[21] A. Paul, R. A. Bartels, R. Tobey, H. Green, S. Weiman, I. P. Christov, M. M. Murnane, H. C. Kapteyn, and S. Backus, "Quasi-phase-matched generation of coherent extreme-ultraviolet light," Nature **421**, 51–54 (2003).

[22] B. Dromey, M. Zepf, M. Landreman, and S. M. Hooker, "Quasi-phasematching of harmonic generation via multimode beating in waveguides," Opt. Express **15**, 7894–7900 (2007).

[23] I. P. Christov, "Propagation of ultrashort pulses in gaseous medium: Breakdown of the quasistatic approximation," Opt. Express **6**, 34–39 (2000).

[24] I. P. Christov, "Control of high harmonic and attosecond pulse generation in aperiodic modulated waveguides," J. Opt. Soc. Am. B **18**(12), 1877–1881 (2001).

[25] A. Bahabad, O. Cohen, M. M. Murnane, and H. C. Kapteyn, "Quasi-periodic and random quasi-phase matching of high harmonic generation," Opt. Lett. **33**, 1936–1938 (2001).

[26]V. Tosa, V. S. Yakovlev, and F. Krausz, "Generation of tunable isolated attosecond pulses in multi-jet systems," New J. Phys. **10**, 025016 (2008).
[27]K. C. Vishnubhatla, N. Bellini, R. Ramponi, G. Cerullo, and R. Osellame, "Shape control of microchannels fabricated in fused silica by femtosecond laser irradiation and chemical etching," Opt. Express **17**, 8685–8695 (2009).
[28]R. Osellame, H. J. W. M. Hoekstra, G. Cerullo, and M. Pollnau, "Femtosecond laser microstructuring: An enabling tool for optofluidic lab-on-chips," Laser Photonics Rev. **5**, 442–463 (2011).
[29]F. He, J. Lin, and Y. Cheng, "Fabrication of hollow optical waveguides in fused silica by three-dimensional femtosecond laser micromachining," Appl. Phys. B **105**, 379–384 (2011).
[30]R. Martínez Vázquez, A. G. Ciriolo, G. Crippa, V. Tosa, F. Sala, M. Devetta, C. Vozzi, S. Stagira, and R. Osellame, "Femtosecond laser micromachining of integrated glass devices for high-order harmonic generation," Int. J. Appl. Glass Sci. **13**, 162–170 (2022).
[31]A. G. Ciriolo, R. Martínez Vázquez, V. Tosa, A. Frezzotti, G. Crippa, M. Devetta, D. Faccialá, F. Frassetto, L. Poletto, A. Pusala, C. Vozzi, R. Osellame, and S. Stagira, "High-order harmonic generation in a microfluidic glass device," J. Phys.: Photonics **2**, 024005 (2020).
[32]E. A. J. Marcatili and R. A. Schmeltzer, "Hollow metallic and dielectric waveguides for long distance optical transmission and lasers," Bell Syst. Tech. J. **43**, 1783–1809 (1964).
[33]S. Hädrich, A. Klenke, J. Rothhardt, M. Krebs, A. Hoffmann, O. Pronin, V. Pervak, J. Limpert, and A. Tünnermann, "High photon flux table-top coherent extreme-ultraviolet source," Nat. Photonics **8**, 779–783 (2014).
[34]S. Hädrich, M. Krebs, A. Hoffmann, A. Klenke, J. Rothhardt, J. Limpert, and A. Tünnermann, "Exploring new avenues in high repetition rate table-top coherent extreme ultraviolet sources," Light: Sci. Appl. **4**(8), e320 (2015).
[35]J. Rothhardt, M. Krebs, S. Hädrich, S. Demmler, J. Limpert, and A. Tünnermann, "Absorption-limited and phase-matched high harmonic generation in the tight focusing regime," New J. Phys. **16**, 033022 (2014).
[36]E. J. Takahashi, Y. Nabekawa, and K. Midorikawa, "Low-divergence coherent soft x-ray source at 13 nm by high-order harmonics," Appl. Phys. Lett. **84**, 4–6 (2004).
[37]E. J. Takahashi, Y. Nabekawa, H. Mashiko, H. Hasegawa, A. Suda, and K. Midorikawa, "Generation of strong optical field in soft X-ray region by using high-order harmonics," IEEE J. Sel. Top. Quantum Electron. **10**, 1315–1328 (2004).
[38]P. Rudawski, C. M. Heyl, F. Brizuela, J. Schwenke, A. Persson, E. Mansten, R. Rakowski, L. Rading, F. Campi, B. Kim, P. Johnsson, and A. L'Huillier, "A high-flux high-order harmonic source," Rev. Sci. Instrum. **84**, 073103 (2013).
[39]A. Cingöz, D. C. Yost, T. K. Allison, A. Ruehl, M. E. Fermann, I. Hartl, and J. Ye, "Direct frequency comb spectroscopy in the extreme ultraviolet," Nature **482**, 68–71 (2012).
[40]I. Pupeza, S. Holzberger, T. Eidam, H. Carstens, D. Esser, J. Weitenberg, P. Rußbüldt, J. Rauschenberger, J. Limpert, T. Udem, A. Tünnermann, T. W. Hänsch, A. Apolonski, F. Krausz, and E. Fill, "Compact high-repetition-rate source of coherent 100 eV radiation," Nat. Photonics **7**, 608–612 (2013).
[41]T. Saule, S. Heinrich, J. Schötz, N. Lilienfein, M. Högner, O. deVries, M. Plötner, J. Weitenberg, D. Esser, J. Schulte, P. Russbueldt, J. Limpert, M. Kling, U. Kleineberg, and I. Pupeza, "High-flux ultrafast extreme-ultraviolet photoemission spectroscopy at 18.4 MHz pulse repetition rate," Nature **10**, 458 (2019).
[42]L. Barreau, A. D. Ross, S. Garg, P. M. Kraus, D. M. Neumark, and S. R. Leone, "Efficient table-top dual-wavelength beamline for ultrafast transient absorption spectroscopy in the soft X-ray region," Sci. Rep. **10**, 5773 (2020).
[43]E. J. Takahashi, T. Kanai, K. L. Ishikawa, Y. Nabekawa, and K. Midorikawa, "Coherent water window x ray by phase-matched high-order harmonic generation in neutral media," Phys. Rev. Lett. **101**, 253901 (2008).
[44]M. Gebhardt, T. Heuermann, R. Klas, C. Liu, A. Kirsche, M. Lenski, Z. Wang, C. Gaida, J. Antonio-Lopez, A. Schülzgen, R. Amezcua-Correa, J. Rothhardt, and J. Limpert, "Bright, high-repetition-rate water window soft X-ray source enabled by nonlinear pulse self-compression in an antiresonant hollow-core fibre," Light: Sci. Appl. **10**, 36 (2021).
[45]G. Fan, K. Legare, V. Cardin, X. Xie, E. Kaksis, G. Andriukaitis, A. Pugzlys, B. Schmidt, J. Wolf, M. Hehn, G. Malinowski, B. Vodungbo, E. Jal, J. Luning, N. Jaouen, Z. Tao, A. Baltuska, F. Legare, and T. Balciunas, "Time-resolving magnetic scattering on rare-earth ferrimagnets with a bright soft-X-ray high-harmonic source," arXiv:1910.14263 (2019).
[46]Y. Fu, K. Nishimura, R. Shao, A. Suda, K. Midorikawa, P. Lan, and E. J. Takahashi, "High efficiency ultrafast water-window harmonic generation for single-shot soft X-ray spectroscopy," Commun. Phys. **3**, 92 (2020).
[47]A. S. Johnson, D. R. Austin, D. A. Wood, C. Brahms, A. Gregory, K. B. Holzner, S. Jarosch, E. W. Larsen, S. S. Parker, C. S. Strüber, P. Ye, J. W. G. Tisch, and J. P. Marangos, "High-flux soft x-ray harmonic generation from ionization-shaped few-cycle laser pulses," Sci. Adv. **4**, eaar3761 (2018).
[48]J. Rothhardt, S. Hädrich, A. Klenke, S. Demmler, A. Hoffmann, T. Gotschall, T. Eidam, M. Krebs, J. Limpert, and A. Tünnermann, "53 W average power few-cycle fiber laser system generating soft x rays up to the water window," Opt. Lett. **39**, 5224–5227 (2014).
[49]T. Auguste, B. Carré, and P. Salières, "Quasi-phase-matching of high-order harmonics using a modulated atomic density," Phys. Rev. A **76**, 011802 (2007).
[50]J. Seres, V. S. Yakovlev, E. Seres, C. Streli, P. Wobrauschek, C. Spielmann, and F. Krausz, "Coherent superposition of laser-driven soft-X-ray harmonics from successive sources," Nat. Phys. **3**, 878–883 (2007).
[51]I. Hadas and A. Bahabad, "Periodic density modulation for quasi-phase-matching of optical frequency conversion is inefficient under shallow focusing and constant ambient pressure," Opt. Lett. **41**, 4000–4003 (2016).
[52]L. D. Landau and E. M. Lifshitz, *Fluid Mechanics* (Pergamon Press, 1987).
[53]COMSOL Multiphysics, version 5.4, www.comsol.com, COMSOL AB, Stockholm, Sweden
[54]C. Cercignani, *Rarefied Gas Dynamics* (Cambridge University Press, 2000).
[55]G. L. Yudin and M. Y. Ivanov, "Nonadiabatic tunnel ionization: Looking inside a laser cycle," Phys. Rev. A **64**, 013409 (2001).
[56]M. Lewenstein, P. Balcou, M. Y. Ivanov, A. L'Huillier, and P. B. Corkum, "Theory of high-harmonic generation by low-frequency laser fields," Phys. Rev. A **49**, 2117 (1994).
[57]P. Paiè, M. Calvarese, F. Ceccarelli, F. Sala, A. Bassi, R. Osellame, F. Bragheri *et al.*, "Integrated fast optical switch fabricated by femtosecond laser micromachining," Proc. SPIE **11991**, 1199105 (2022).
[58]R. Pol, F. Céspedes, D. Gabriel, and M. Baeza, "Microfluidic lab-on-a-chip platforms for environmental monitoring," Trends Anal. Chem. **95**, 62–68 (2017).
[59]H. Shi, K. Nie, B. Dong, M. Long, H. Xu, and Z. Liu, "Recent progress of microfluidic reactors for biomedical applications," Chem. Eng. J. **361**, 635–650 (2019).
[60]X. Cheng, M. D. Ooms, and D. Sinton, "Biomass-to-biocrude on a chip via hydrothermal liquefaction of algae," Lab Chip **16**(2), 256–260 (2016).
[61]T. Salditt and M. Osterhoff, "X-ray focusing and optics," Nanoscale Photonic Imaging **134**, 71–124 (2020).
[62]T. Salditt, S. Hoffmann, M. Vassholz, J. Haber, M. Osterhoff, and J. Hilhorst, "X-ray optics on a chip: Guiding x rays in curved channels," Phys. Rev. Lett. **115**, 203902 (2015).
[63]A. Crespi, Y. Gu, B. Ngamsom, H. J. W. M. Hoekstra, C. Dongre, M. Pollnau, R. Ramponi, H. H. van den Vlekkert, P. Watts, G. Cerullo, and R. Osellame, "Three-dimensional Mach-Zehnder interferometer in a microfluidic chip for spatially-resolved label-free detection," Lab Chip **10**, 1167–1173 (2010).
[64]L. Poletto, G. Tondello, and P. Villoresi, "High-order laser harmonics detection in the EUV and soft x-ray spectral regions," Rev. Sci. Instrum. **72**, 2868–2874 (2001).
[65]The Center for X-Ray Optics (CXRO), https://henke.lbl.gov/optical_constants/.
[66]L. Poletto, G. Naletto, and G. Tondello, "Grazing-incidence flat-field spectrometer for high-order harmonic diagnostics," Opt. Eng. **40**, 178–185 (2001).
[67]Available Online: https://www.princetoninstruments.com/products/pixis-family/pixis-xo.